LAWRENCE
LIVERMORE
NATIONAL
LABORATORY

LLNL-JRNL-408645

Quantification of radiation induced crosslinking in a commercial, toughened silicone rubber, TR-55, by 1H MQ-NMR

R. Maxwell, S. Chinn, C. Alviso, C. A. Harvey, J. Giuliani, T. Wilson, R. Cohenour

November 13, 2008

Polymer Degradation and Stability

Disclaimer

Quantification of radiation induced crosslinking in a commercial, toughened silicone rubber, TR-55 by ^{1}H MQ-NMR

Robert S. Maxwell[*], Sarah C. Chinn[1], Cynthia T. Alviso[1], Chris A. Harvey[1], Jason R. Giuliani,[3] Thomas S. Wilson[1], Rebecca Cohenour[2]

[1]Lawrence Livermore National Laboratory, Livermore, CA 94551
[2]Honeywell Federal Manufacturing and Technology, Kansas City Plant, Kansas City, MO 64141

Abstract

Radiation induced degradation in a commercial, filled silicone composite has been studied by SPME/GC-MS, DMA, DSC, swelling, and Multiple Quantum NMR. Analysis of volatile and semivolatile species indicates degradation via decomposition of the peroxide curing catalyst and radiation induced backbiting reactions. DMA, swelling, and spin-echo NMR analysis indicate a increase in crosslink density of near 100% upon exposure to a cumulative dose of 250 kGray. Analysis of the sol-fraction via Charlseby – Pinner analysis indicates a ratio of chain scission to crosslinking yields of 0.38, consistent with the dominance of the crosslinking observed by DMA, swelling and spin-echo NMR and the chain scissioning reactions observed by MS analysis. Mulitple Quantum NMR has revealed a bimodal distribution of residual dipolar couplings near 1 krad/sec and 5 krad/sec in an approximately 90:10 ratio, consistent with bulk network chains and chains associated with the filler surface. Upon exposure to radiation, the mean $\langle\Omega_d\rangle$ for both domains and the width of both domains both increased. The MQ NMR analysis provided increase insight into the effects of ionizing radiation on the network structure of silicone polymers.

Introduction

PolyDiMethylSiloxane (PDMS) composite systems can be synthesized by the use of any of a large variety of synthetic pathways to produce a broad range of network topologies.[1, 2] When formulated with reinforcing filler phase such as silica or carbon black, the resulting composites have a broad range of realizable physical properties [3]. Unsurprisingly, a number of commercial formulations now exist tailored for use in a number of specific scientific and technological applications, including aerospace, electrical, sealant, adhesive, personal care, and medical industries.

The specific degradation pathways (crosslinking, backbiting, unzipping, etc.) might be expected to be similar for the dominant silicone formulations. The dominant aging mechanisms have recently been reviewed by Carlson, et al. [6]. Pioneering work on radiation effects on linear siloxanes by Charlesby and Miller that demonstrated that radiation exposure produced primarily crosslinking reactions proportional to cumulative dose [4, 5]. Further work on both soluble polymers and insoluble elastomeric networks, has shown that chain scission can occur, though typically to a lesser extent than crosslinking and that a number of volatile and semi-volatile species are released as a result of radiation induced chemical processes [6-11]. The presence of phenyl groups and filler particles have been shown to have varying effects on degradation [12-13].

Unfortunately, the effect of these degradation mechanisms on the network structure and filler reinforcement mechanisms, and the resulting mechanical properties, are expected to vary from formulation to formulation due to the large variability in network structure and filler content. A number of spectroscopic and analytical methods exist for assessing degradation based on signatures from the lower molecular weight fragments produced from the degradation or from measurement of the significant

speciation changes resulting from degradation. Gel-Permeation Chromatography and solution state NMR methods, for example, will only provide insight into the changes occurring in the soluable sol-fraction. FTIR and standard Magic Angle Spinning ^{13}C, ^{29}Si, or ^{1}H NMR can provide insight into the chemical speciation changes in the bulk materials if they are significant enough to produce signatures in sufficient quantity. Head space analysis by various Mass Spectrometry based methods can provide insight into volatile or semi-volatile degradation by products, but provides no insight into the remaining polymer network topology. Unfortunately, for numerous polymer systems, including network silicones, there are few methodologies that allow for the direct investigation of the aging mechanisms and their resulting effect on the network structure, specifically the distributions of chain lengths. Standard mechanical property measurements provide key insight into the effects of degradation on the physical properties, but do not, generally, provide structural insight into the network structure without correlation to a chosen network theory model.

Recently, static ^{1}H Mulitple Quantum NMR has shown remarkable ability to provide insight into the changes in network structure due to degradation.[14-16] ^{1}H MQ NMR allows the quantification of the residual dipolar couplings resulting from incomplete averaging of the homo-nuclear dipolar couplings between protons in the network due to restricted, anisotropic motion locked in by the physical and chemical contraints (e.g. crosslinks and entanglements), as illustrated in **Figure 1**. The relationship between the residual dipolar coupling and polymer structural variables has been described in a number of other reports. [17-22] These studies have correlated the residual

dipolar couplings to the dynamic order parameter, S_b, and to the number of statistical segments, N, between constraints:

$$S_b = \frac{1}{P_2(\cos\alpha)} \frac{\langle \Omega_d \rangle}{\langle \Omega_d \rangle_{static}} = \frac{3r^2}{5N} \qquad \{1\}$$

where $\langle \Omega_d \rangle_{static}$ is the dipolar coupling in the absence of motion, $\langle P_2(\cos\alpha) \rangle$ is the time-averaged second order Legendre polynomial of the angle between the dipolar vector and the chain axis, and r is the vector describing the deviation of the end-to-end vector, **R**, from that of the unperturbed melt, $\mathbf{R}_o$: $r=\mathbf{R}/\mathbf{R}_o$. Recent work by Saalwächter has shown that quantitative equivalence between S_b and the crosslink density can be made in certain cases.[22]

In this paper, we report the use of ^{1}H MQ-NMR to assess the changes in a commercial silicone formulation, TR55, due to exposure to γ-radiation from a Co-60 source. TR55 is composed of 70 wt. % polysiloxane gum formulation and 30 wt. % fumed silica filler pretreated with a proprietary silating agent. This formulation finds uses in the aviation and food processing industries, among others. Due to the service requirements in such applications, there is significant interest in understanding the mechanisms and effects of degradation of TR55 is hostile environments of either ionizing radiation or elevated temperature. The NMR data is complimented by more standard techniques, including DMA, DSC, GPC, and Solid-Phase MicroExtraction (SPME) GC/MS analysis of the headspace gasses.

Experimental

2.1 Materials Preparation: TR-55 gum stock was obtained from Dow Corning and cured by mixing with DiCup40 peroxide curing agent. TR55 is known to be composed of 30 wt% silica filler, ~70 wt. % silicone gum stock, and ~ 0.6 wt% lithium stearate processing aid. The silicone gum stock is approximately 97.5 wt.% PDMS, 2 wt. % polymethylsilane, and 0.4 wt.% polymethylvinylsiloxane. Twenty sample strips (700mm x 130mm x 20mm each) of TR55 were then placed into a stainless steel vessel (sealed) and exposed to a 1.2 MeV, 5kGray/hour, C-60 source and irradiated to 10 kGray to 250 kGray. Four remaining samples to be analyzed in the pristine state and were set aside.

2.2 Solvent swelling: Details of the two stage solvent swelling procedure used here has been reported elsewhere, but is briefly repeated here [10, 11, 23]. The crosslink density in the bulk polymer matrix was obtained by initially submerging in 600 ml of toluene in a Teflon container (~ 1-3 days to reach equilibrium). The swollen weight was recorded and 150 ml of concentrated NH_4OH (~28%) was added directly to the toluene solution. The samples were then weighed periodically until equilibrium was reached with the toluene/NH_4OH mixture. The additional swelling yields the contribution to the crosslink density of the hydrogen bonds between the silica filler and the polymer chains. The samples were dried overnight in a vacuum oven at ambient temperature and reweighed for the final dry weight. Molecular weights between crosslinks (MW_i) and crosslink densities (ν_i) were then calculated using the Flory and French equations [24, 25]. The molecular weight determined in toluene was defined as the total molecular weight between crosslinks, MW_{total}. The molecular weight determined from swelling in the toluene/NH_4OH mixture was defined as the molecular weight between crosslinks in the

polymer network, MW_{poly}. The difference was the defined as the contribution of the molecular weight due to interactions between the polymer and the filler.

$$MW_{poly} = MW_{total} + MW_{filler} \quad \{2\}$$

The crosslink densities, ν_{poly}, ν_{total}, and ν_{filler}, were determined using equation (3):

$$\nu_i = MW_{monomer}/MW_i \quad \{3\}$$

2.3 DMA: DMA testing was performed (TA Instruments AR2000 Rheometer, New Castle, Delaware) in parallel plate geometry. Specimens were disks approximately 2 mm in thickness and 8 mm in diameter. The sample was sheared at a frequency of f = 6.3 rad/sec. For room temperature shear storage modulus measurements, samples were sheared up to 1% strain level with a static compression force of 1 N. Isothermal cold crystallization experiments were performed by cooling the sample down to -85 °C and dwelling at this temperature for 3 to 4 hours. A static normal force of 4 N was placed upon the sample and shear strain was kept constant at 0.5%.

2.4 DSC: Differential Scanning Calorimetry experiments were performed on a TA Instruments Q1000 DSC. Approximately 10-15 mg of sample was sealed in an aluminum pan and the samples were subjected to a modulated 1.5 ºC/min temperature ramp from -160 ºC to -90 ºC with a temperature modulation of ± 0.80 ºC every 80 seconds under a Helium purge with a flow rate of approximately 50 mL/min. The temperature modulation was then changed to ± 0.10 ºC every 80 seconds until the maximum temperature of -10 ºC was reached. The temperature modulation rate was set to increase

the sensitivity of the instrument for measurement of the glass transition temperature and subsequently to increase the accuracy for the melt temperature measurement.

2.5 Solid Phase Micro Extraction (SPME) Materials: Once the appropriate radiation dose was achieved, the samples were removed from the vessel and 150 samples were prepared weighing 20-30 mg each. These samples were placed in SPME headspace vials (20mL), and sealed with crimp caps and septa (20mm, teflon/blue silicone, level 4) that were purchased from MicroLiter Analytical Supplies. For each dose, five were left at room temperature, five were placed in a 70˚C oven, and five were placed in a 150˚C oven. All samples remained at their designated temperatures for two weeks. An additional set of blanks (sealed empty vials) was prepared for storage at room temperature, 70˚C, and 150˚C prior to SPME sampling. The storage at elevated temperatures was performed to maximize the volatilization of degradation signatures for observation by SPME sampling, while retaining a room temperature sample and a blank to serve as controls.

Fifteen samples weighing 20-30 mg each were also prepared in glass tubes (180mm x 10mm), backfilled with nitrogen and flame sealed. (A blank tube was prepared in the same manner for each dose.) These samples were exposed to identical irradiation conditions as the samples prepared in plastic bags. All samples and blanks were then left at room temperature prior to sampling with SPME. (Additional thermal treatments were not performed.) In order to collect the headspace sample in-situ, the glass tube was placed within another custom made, baked out, glass tube with airtight fittings at each end. One end contained a sharpened steel rod and the other a 20mm, teflon/blue level 4 septa. By striking the steel rod, the sample glass would break allowing

the headspace to escape into the outer glass tube. The SPME needle was then inserted into the opposite end through the septa, the fiber extended and exposed for 10 minutes. The fiber was then retracted, the needle removed and manually inserted into the GC for analysis.

Samples were analyzed by SPME GC/MS using an Agilent 6890 GC-5973 MSD system. Volatile species were captured on an 85 μm Carboxen/PDMS SPME fiber (purchased from Supelco). Each headspace was sampled at 50˚C for 20 minutes and injected into the GC for one minute at 250˚C. The fiber was conditioned between each sample for five minutes at 260˚C. The Agilent 6890 GC was run in splitless mode with the purge vent opening at 0.5 minutes. Chromatographic separation was achieved using a J & W Scientific DB-624 column (30 m, 0.25 mm ID, 1.4 μm film) with a 1.0 mL/min constant flow of helium. The GC oven temperature was held at 40˚C for 1.05 min. and then programmed to 260˚C at a rate of 23.41˚C/min, with a final hold of 6.81 min. The Agilent 5973 mass spectrometer scanned the mass range from 35-450 at a rate of 1.81 scans/s with no filament delay. Outgassing products were identified by comparison of their mass spectra to the NIST 02 mass spectral library.

2.6 NMR Methods: All static NMR experiments were performed on a Bruker Avance 400 spectrometer with a ^{1}H frequency of 400.13 MHz. Samples with dimensions (3 mm x 3 mm x 2 mm) were centered within the coil volume of a Bruker TBI (HCX) 5 mm probe with 90^{o} pulse lengths $\tau_p = 4.50$ μs. Traditional ^{1}H Hahn-spin echo experiments, using the pulse sequence shown in **Figure 2A**, were performed as previously described [10, 11, 14, 23] with recycle delay times of 6-10 s. Multiple Quantum NMR experiments were

performed as described previously by us [14-16] and by Saalwächter et al. [19-22] using the generic pulse sequence shown in **Figure 2B** to excite even-quantum coherences. Reference spectra, containing all excited 4n quantum orders, were collected using the DQ selection phase cycle without receiver alternation. All experiments were preformed by incrementing the DQ mixing time ($\tau_{DQ}=a(\psi)n_c t_c$) with cycle times (t_c) of 180 μs and the finite nature of the rf pulses compensated for using the scaling factor $a(\psi)=1-12*(\tau_p/t_c)$ rigorously derived elsewhere. [19]

Results and Discussion:

Typical SPME sampled GC/MS chromatograms are shown in **Figure 3** for samples sampled directly after irradiation without heating and with thermal treatments at 70 and 150 ºC. **Table 1** lists the predominant species observed. Two different analysis methods were employed: a so-called "in-situ" method where the offgassing species were preferentially observed by directly sampling the headspace after irradiation, and the "bulk" method where the analysis was performed directly on the irradiated material after removing it from its irradiation environment. The "in-situ" chromatogram of the pristine sample held at room temperature displays two small peaks assigned to isopropyl alcohol and trimethylsilanol. Upon irradiation, these peaks grew significantly, possibly due to post-cure reactions and degradation of either a trimethylsilyl endcapped polymer chain or trimethylsilyanol groups from the silica filler. At high dose, several additional peaks also appeared. These are attributed to low molecular weight species preferentially observed by direct sampling (propane, isobutane, butane, and ethanol) and are likely due to degradation of the dicumyl peroxide curing agent and the lithium stearate processing aid since no propyl or aromatic groups have been observed by NMR, IR or MS analysis of

the uncured gum stock. An additional peak attributed to trimethylsilyl fluoride is likely due to a reaction of the large amount of trimethylsilanol with fluorine in the Teflon septum. Finally, the appearance of trimethylmethyoxysilane is likely due to a methylation of the trimethylsilanol, resulting in an extremely volatile offgassing species.

Traditional SPME analysis of the bulk material (after it had been removed from the irradiation bags and placed in a SPME vial) revealed mostly higher molecular weight cyclic siloxanes. These are likely the result of radiation induced backbiting reactions observed in previous studies of radiation induced degradation of siloxane polymers.[6, 26-40] It has been postulated that recombination of the two types of polymer radicals >Si• and >$SiCH_2$• can lead to three types of crosslinks [30]. No direct observation, however, of the any of these potential crosslink species has been obtained by NMR or IR, likely due to the small number of crosslinks formed. At high doses, lower molecular weight cyclic and linear siloxanes appeared, indicating further degradation of the material.

It is interesting to note that the isopropanol and trimethyl silanol that were present in the "in-situ" samples were only seen in the "bulk" sample with the combined irradiation and heat treament, while the siloxanes were only barely observable in the "in-situ" samples. These drastic differences in chromatograms can mainly be attributed to differences in sampling procedures. The SMPE vials with the "bulk" material were placed in a 50º heater for 20 minutes while the sampling was taking place, while the materials in the "in-situ" apparatus were sampled on the bench top at room temperature for 10 minutes. An increase in SPME sampling time typically leads to an increase in signals for materials with longer elution times. Further, the bulk samples were not only

sampled longer, but they also were sampled at elevated temperature, which would likely result in greater volatilization of the cyclic siloxanes. This was confirmed in a pristine, in-situ sample that was held at 70ºC (data not shown here). The combined effect of the sample treatment meant that the "in-situ" method was preferentially detecting signatures with shorter elution times, which accentuated the naturally large intensity of the volatile alcohols. The "bulk" sampling method does not directly sample the headspace, so these species did not appear in the low-dose or low-temperature conditions. With the combined radiation and thermal treatment, however, large amounts of these species were observed.

Results of swelling and DMA analysis are shown in **Figure 4** for the pristine and irradiated TR55 samples. All three methods show evidence for the dominance of crosslinking reactions. The molecular weight between crosslinks obtained from solvent swelling as a function of cumulative dose is shown in **Figure 4A**. For all three measured molecular weights, polymer, polymer-filler, and total, an increase in ν_i was observed with increasing cumulative dose with exposure up 250 kGray leading to an increase in the crosslink density of about 100%. Changes in shear modulus obtained by ambient DMA analysis are shown in **Figure 4B** and indicate that as the materials were exposed to increasing cumulative dose the modulus was observed to increase from 4 to 8.1 MPa – a 100% increase consistent with the swelling results as expected from polymer network theory ($G \sim \nu_i$) [41].

Spin-echo decay curves for the samples exposed to radiation are shown in **Figure 5**. The decay curves are characterized by a mixed Gaussian-exponential decay typical of elastomers above their glass transition temperature and are due to the effects of motional

constraints caused by physical and chemical constraints [17]. Changes in the effective Spin-echo, transverse ^{1}H relaxation times (T_{2e}) obtained simply from the point at which the intensity decayed to 1/e of the initial intensity are shown in **Figure 5B** and indicate that increased cumulative dose resulted in an increase in the relaxation rate ($1/T_2$).

More accurate quantification of the residual dipolar couplings are obtained from fitting the decay of a echo to the equation for echo decay in the presence of anisotropic motion due to topological constraints, as has been shown elsewhere: [23]

$$E(t) = X_{short} * \exp\left(-\frac{t}{T_2} - \left\langle \Omega_d^2 \right\rangle \tau_s^2 \left[\exp\left(\frac{t}{\tau_s}\right) + \frac{t}{\tau_s} - 1\right]\right) + X_{long} * \exp\left(-\frac{2t}{T_{2long}}\right) \quad \{4\}$$

where X_i are the mole fractions of chains in each domain, τ the delay between the 90° and 180° pulses, τ_s is the correlation time for the motions associated with the residual dipolar couplings, and T_{2i} are the transverse relaxation time in the absence of residual dipolar couplings (i.e. the T_2 of the sol-fraction). The first term on the right side of equation {4} is typically assigned to the polymer chains associated with the crosslinked network while the domains with the long T_2 are assigned to the chains associated with the uncrosslinked, sol-fraction.[11, 17, 23] Extraction of the mean squared average of the residual dipolar couplings $\langle\Omega_d\rangle^2$ from fits of the spin-echo decay curves to equation {4} are shown in **Figure 5C** and show similar trends to the swelling, DMA, and simple analysis of the relaxation rates. From equation {1}, the change of 110 % in $1/T_2$ and $\langle\Omega_d\rangle^2$ derived from the spin-echo analysis is also consistent with the changes observed in crosslink density.

As can be seen in **Figure 5A**, the % of the spin-echo decay curve due to the long relation time component (the sol-fraction) was observed to be dose dependent. The sol-fraction, S, was determined for all samples from extrapolation to t=0 of this component. A plot of $S + \sqrt{S}$ as a function of $(Dose)^{-1}$ (so-called Charlseby-Pinner plot) is shown in **Figure 6.** The trend for the samples studied here is significantly non-linear, reflecting the deviation of the polymer network chains from a random distribution also observed in the MQ-NMR, as discussed below [40]. Extrapolating the curve in **Figure 6** to infinite dose, one obtains a ratio of G_s/G_x of ~ 0.38 ± 0.02 This ratio is similar to ratio's obtained for other studies of silicone materials. [42, 47, 48]

A decrease in segmental mobility with cumulative dose revealed in the spin echo results should be observable by changes in the molecular mobility as measured by thermal analysis methods. Filled silicone composites are known to crystallize over a range of temperatures that depend on their network structure – including the crosslink density, the number and type of crosslinks, the content of phenyl siloxane monomers (here none as indicated by ^1H MAS NMR), and the filler content and interaction with the polymer chains. DSC analysis of TR55 indicates a crystallization at -70 ºC on cool down and melts at -45 ºC on heating. DSC characterization of irradiated samples indicates a decrease in T_m and the heat of fusion, ΔH_m with increasing dose, as shown in **Figure 7,** though no change in the glass transition temperature. The decrease in T_m and ΔH_m suggest that the PDMS chains are prevented from crystallizing, likely due to the increase in crosslink density reducing the segmental dynamics of the chains.

The swelling, DMA, DSC, and spin-echo NMR data are all consistent with the dominance of radiative induced crosslinking mechanisms over chain scission reactions.

The trends with cumulative dose are nearly linear over the range of doses studied. These methods, however, provide only bulk average measurements with no detailed assessment of distributions within the network structure. To gain further insight into the changes between network structural motifs, we employed static ^{1}H MQ-NMR. Growth curves for the TR55 samples are shown in **Figure 8** and show that as the exposure increased the growth rate increased steadily, consistent with an increase in the average residual dipolar coupling with cumulative dose. The DQ build-up curves were normalized as described previously. [14-22]

The dipolar couplings contributing to the normalized DQ build-up curve were extracted within the second-moment approximation as a summation of growth curves

$$I_{DQ}(\langle\Omega_d\rangle;\tau_{DQ}) = \sum X(\Omega_i) * 0.5 * (1 - e^{-\frac{2}{5}\langle\Omega_d\rangle_i^2 \tau_{DQ}^2}) \qquad \{5\}$$

where $X(\Omega_i)$ is the relative mole fraction of spins. For the samples studied here, a Gaussian distribution around two RDCs were assumed resulting in a growth curve equation:

$$I_{nDQ}(\tau_{DQ}) = 0.5 * \sum_{i=1}^{n} X_i * \left[1 - \frac{e^{\frac{-<\Omega_d>_i^2 \tau_{DQ}^2}{1+\frac{4}{5}\sigma_{d,i}^2 \tau_{DQ}2}}}{\sqrt{1+\frac{4}{5}\sigma_{d,i}^2 \tau_{DQ}2}} \right] \qquad \{6\}$$

where $\sigma_{d,i}$ is the width for the distribution with mean $<\Omega_d>_i$ [20]. A two site model was used (i.e. n=2) here. Fits of the MQ growth curves to equation {6} are also shown **in Figures 7**. Fits to one $<\Omega_d>$ using equation {5} or one distribution of $<\Omega_d>$ using equation {6} with N=1 did not sufficiently reproduce the growth curves. A superposition two Gaussian distributions of $<\Omega_d>$ were needed to obtain reasonable fits to the data. Analysis of the MQ growth curves by regularization [data not shown], as has been done

previously for other silicones, produced similar distribution profiles [14,21]. The data could not be fit reasonably to a Gamma function distribution that would be predicted for a Gaussian distribution of end-to-end vectors [19].

The resulting distributions using the fitting parameters from equation {6} are shown in **Figure 8**. The distributions show two populations of mean $<\Omega_d>$, centered at about 1 krad/sec and 3 krad/sec. The first domain assigned to network chains with a low crosslink density (more mobility) and the second domain is assigned to network chains with a higher crosslink density (less mobility). Given what we know about the network structure of TR55 (i.e. crosslinks are obtained only through tetra-functional sites and the chain lengths are relatively monodisperse), we assign this domain to network chains associated with the filler surface. Other studies have shown that adsorbed PDMS chains on silica surfaces are described by elevated $<\Omega_d>$. [14, 15, 23, 43]

The mean $<\Omega_d>$ for both domains and the distribution widths were observed to increase with increasing cumulative dose, as shown in Figure 8. The average $<\Omega_d>$ and σ_d are also plotted as a function of exposure in **Figure 9**. The distributions show a general increase in $<\Omega_d>_{low}$ and $<\Omega_d>_{high}$ with increasing dose, consistent with the spin-echo, DMA, and swelling data. The distributions, however, also indicate that broadening in the widths of the distributions at increasingly higher exposures. Broadening of chain length distributions with crosslinking reactions has been predicted by numerous studies of chain statistics in soluble linear polymers and reflects the simultaneous occurrence of both crosslinking and chain scissioning mechanisms.[45-46]

Conclusions:

We have studied the radiation induced degradation in a commercial filled silicone elastomer, TR55, by solvent swelling, DMA, and NMR techniques. Standard swelling, DMA and ^{1}H spin-echo experiments confirmed that exposure to γ-radiation caused primarly crosslinking reactions that approximately double the crosslink density with exposures of 250 kGray. Unfortunately, these methods provide only a bulk measure of the average change in polymer chain structure. Static ^{1}H MQ-NMR was used to obtain the distribution of the chain network structure and the changes that occurred due to exposure to radiation. The MQ-NMR results indicate that the network structure of TR55 could be described by a Gaussian distribution of $<\Omega_d>$ for both the network chains and the chains associated to the filler surface. For both domains, exposure to radiation caused an increase in $<\Omega_d>$, e.g. an increase in the crosslink density, and an increase in the width of $<\Omega_d>$, e.g. an increase in the breadth of crosslink densities, in agreement with previous generic predictions of chain statistics.[45-46] Since the stress response of silicone networks will depend on both the average crosslink density, but also on the distribution of crosslink densities, the such insight can provide increased understanding of the mechanisms that lead to material performance changes over time.

Acknowledgements:

We thank the following for generous help in the course of this work: Erica Gjersing, Julie Herberg, Kay Saalwächter, and Ticora Jones. Portions of this work were performed under the auspices of the Department of Energy by Lawrence Livermore National Laboratory under contract DE-AC52-07NA27344. Financial support from the

LLNL Laboratory Directed Research and Development (LDRD) program (005-SI-06) is acknowledged.

References:

[1] Brook MA. Silicon in Organic, Organometallic and Polymer Chemistry. John Wiley 2000. New York, NY.

[2] Erman B, Mark JE. Structures and Properties of Rubberlike Networks. Oxford Univ Press 1997. New York, NY.

[3] Nielsen LE, Landel RF. Mechanical Properties of Polymers and Composites, 2nd edition. CRC Press 1994. New York, NY.

[4] Charlesby A. Changes in silicone polymeric fluids due to high energy radiation. Proc Roy Soc 1955;A230(1180):120-135.

[5] Miller AA. Radiation chemistry of polydimethylsiloxane, crosslinking and gas yields. J Amer Chem Soc 1960;82:3519-3523.

[6] Palsule AS, Clarson SJ, Widenhouse CW. Gamma irradiation of silicones. J Inorg Organomet Polym 2008;18:207–221.

[7] Warrick EL. Effect of radiation on organopolysiloxanes. Ind Eng Chem 1955;24:842-848.

[8] Basfar AA. Hardness measurements of silicone rubber and polyurethane rubber cured by ionizing radiation. Radiat Phys Chem 1997;50:607-610.

[9] Mark JE, McCarthy DW. Poly(dimethylsiloxane) elastomers from aqueous emulsions: III. Effect of blended silica fillers and gamma-radiation-induced crosslinking. Rubber Chem Tech 1998;71:941-948.

[10] Chien A, Maxwell R, Chambers D, Balazs B, LeMay J. Characterization of radiation-induced aging in silica-reinforced polysiloxane composites. Rad Phys Chem 2000;59:493–500.

[11] Maxwell R, Cohenour R, Sung W, Solyom D, Patel M. The effects of gamma-radiation on the thermal, mechanical, and segmental dynamics of a silica filled room temperature vulcanized polysiloxane rubber. Polym Degrad Stab 2003;80:443–450.

[12] Burlant W, Serment V, Neerman J. Gamma-radiation of para-substituted polystyrenes. J Polym Sci 1962;58:491-502.

[13] Mark JE. Physical Properties of Polymers Handbook. Amer Inst Phys Press 1996. New York, NY.

[14] Maxwell RS, Chinn SC, Solyom D, Cohenour R. Radiation-induced cross-linking in a silica-filled elastomer as investigated by multiple quantum ^{1}H NMR. Macromolecules 2005;38:7026-7032.

[15] Chinn S, DeTeresa S, Sawvel A, Shields A, Balazs B, Maxwell RS. Chemical origins of permanent set in a peroxide cured filled silicone elastomer - tensile and ^{1}H NMR analysis. Polym Degrad Stab 2006;91:555-564.

[16] Giuliani JR, Gjersing EL, Chinn SC, Jones TV, Wilson TS, Alviso CT, Herberg JL, Pearson MA, Maxwell RS. Thermal degradation in a trimodal poly(dimethylsiloxane) network studied by multiple quantum ^{1}H NMR. J Phys Chem 2007; B111:12977-12984.

[17] Cohen Addad JP. NMR and fractal properties of polymeric liquids and gels. Progr NMR Spectrosc 1993;25:1-316.

[18] Schmidt-Rohr K, Spiess HW, Multidimensional Solid-State NMR and Polymers, Academic Press 1994. San Diego, CA.

[19] Saalwächter K. Proton multiple-quantum NMR for the study of chain dynamics and structural constraints in polymeric soft materials. Progr NMR Spectrosc 2007;51:1-35.

[20] Saalwächter K, Ziegler P, Spyckerelle O, Haidar B, Vidal A, Sommer JU. ^{1}H multiple-quantum nuclear magnetic resonance investigations of molecular order distributions in poly(dimethylsiloxane) networks: evidence for a linear mixing law in bimodal systems. J Chem Phys 2003;119:3468-3482.

[21] Saalwächter K, Heuer A. Chain dynamics in elastomers as investigated by proton multiple-quantum NMR. Macromolecules 2006;39:3291-3303.

[22] Saalwächter K, Herrero B, Lopez-Manchado MA. Chain order and cross-link density of elastomers as investigated by proton multiple-quantum NMR. Macromolecules 2005;38:9650-9660.

[23] Maxwell RS, Balazs B. Residual dipolar coupling for the assessment of cross-link density changes in gamma-irradiated silica-PDMS composite materials. J Chem Phys 2002;116:10492-10502.

[24] French DM. Crosslink density and solvent swelling of filled and unfilled stocks. J Appl Poly Sci 1980;25:665-682.

[25] Vondracek P, Pouchelon A. Ammonia-induced tensile set and swelling in silica-filled silicone-rubber. Rubber Chem Technol 1990;63:202-214; Flory PJ. Principles of Polymer Chemistry. Cornell Univ Press 1953. Ithaca, NY.

[26] Tanny GB, St Pierre LE. Production of cyclic molecules during gamma-irradiation of linear polydimethylsiloxane. J Polym Sci Polym Lett 1971;9:863-868.
[27] Evans D, Crook M. Irradiation of plastics: damage and gas evolution. MRS Bulletin 1997;22:36-46.
[28] Chahal RS, St Pierre LE. Radiation induced bonding of hexamethyldisiloxane to silica. Canad J Chem 1969;47:2311-2314.
[29] Delides CG, Shepherd IW. Dose effects in crosslinking of irradiated polysiloxane. Rad Phys Chem 1977;10:379-385.
[30] Miller AA. Radiation chemistry of polydimethylsiloxane. 1. Crosslinking and gas yields. J Amer Chem Soc 1960;82:3519-3523.
[31] Menhofer H, Zluticky J, Heusinger H. The influence of irradiation temperature and oxygen on crosslink formation and segment mobility in gamma-irradiated polydimethylsiloxanes. Rad Phys Chem 1989;33:561-566.
[32] Litvinov VM, De PP. Spectroscopy of Rubbers and Rubbery Materials. Rapra Technology Ltd. 2002. Shawbury, UK.
[33] Chang CL, Don TM, Lee HSJ, Sha YO. Studies on the aminolysis of RTV silicone rubber and modifications of degradation products. Polym Degrad Stab 2004;85:769-777.
[34] Mitra S, Ghanbari-Siahkali A, Almdal K. A novel method for monitoring chemical degradation of crosslinked rubber by stress relaxation under tension. Polym Degrad Stab 2006;91:2520-2526.
[35] Celina M, Trujillo AB, Gillen KT, Minier LM. Chemiluminescence as a condition monitoring method for thermal aging and lifetime prediction of an HTPB elastomer. Polym Degrad Stab 2006;91:2365-2374.
[36] Hall AD, Patel M. Thermal stability of foamed polysiloxane rubbers: Headspace analysis using solid phase microextraction and analysis of solvent extractable material using conventional GC-MS. Polym Degrad Stab 2006;91:2532-2539.
[37] Zhou WJ, Yang H, Guo XZ, Lu JJ. Thermal degradation behaviors of some branched and linear polysiloxanes. Polym Degrad Stab 2006;91:1471-1475.
[38] Zlatevich L. Luminescence Techniques in Solid State Polymer Research. Marcel Dekker 1989. New York, NY.
[39] Celina M, Clough RL, Jones GD. Initiation of polymer degradation via transfer of infectious species. Polym Degrad Stab 2006;91:1036-1044.
[40] Ashby GE. Oxyluminescence from polypropylene. J Polym Sci 1961;50:99-112.
[41] Ferry JD. Viscoelastic Properties of Polymers, 3rd edition. John Wiley 1980. New York, NY.
[42] Charlesby A, Pinner SH. Analysis of the solubility behaviour of irradiated polyethylene and other polymers. Proc Roy Soc 1959;A249:367-386.
[43] Wang M, Bertmer M, Demco DE, Blumich B, Litvinov VM, Barthel H. Indication of heterogeneity in chain-segment order of a PDMS layer grafted onto a silica surface by ^{1}H multiple-quantum NMR. Macromolecules 2003;36:4411-4413.
[44] Tobita H, Yamamoto Y, Ito K. Molecular-weight distribution in random cross-linking of polymers – modality of the molecular-weight distribution. Macromol Theor Simul 1994;3:1033-1049.
[45] Kimura T. Molecular weight distribution of irradiated polymers. J Phys Soc Japan 1962;17:1884-1896.
[46] Maiti A, Gee R, Chinn S, **Maxwell RS**, Constitutive modeling of Radiation effects on the Permanent Set in a silicone elastomer, Polym. Degrad. Stab. *(*2008) in press

Tables:
Table 1: Species observed by SPME-GC/MS analysis.

Code	Retention Time (min)	Species
A	4.329	Isopropyl alcohol
B	5.081	Trimethylsilanol
C	5.489	Hexamethyl disiloxane
D	6.752	Hexamethyl cyclotrisiloxane
E	6.919	Trans-(2-chlorovinyl) dimethylethoxysilane
F	8.246	Octamethyl cyclotetrasiloxane
G	10.270	Dodecamethyl cyclohexasiloxane
H	11.338	Tetradecamethyl cycloheptasiloxane
I	12.563	Hexadecamethyl cyclooctasiloxane
a	2.881, 3.075, 3.270	Propane, Isobutane, Butane
b	3.438	Trimethylsilylfluoride
c	3.957	Ethanol
d	4.552	Trimethyl methyoxysilane

Figure 1. Illustration of motional processes occurring in silicone polymers that dominate residual dipolar couplings between proton within methyl side groups. Rapid motion around C_3 axis of Si-CH_3 bond preaverages $\langle\Omega_d\rangle$ to ~ 1/3 of $\langle\Omega_d\rangle_{static}$ of 8900 Hz (A). Slower, motion restricted by nearby physical and chemical constraints (enganglements and crosslinks) further reduces $\langle\Omega_d\rangle$ to a level that is dependent on the chain length, as described by equation {1} (B).

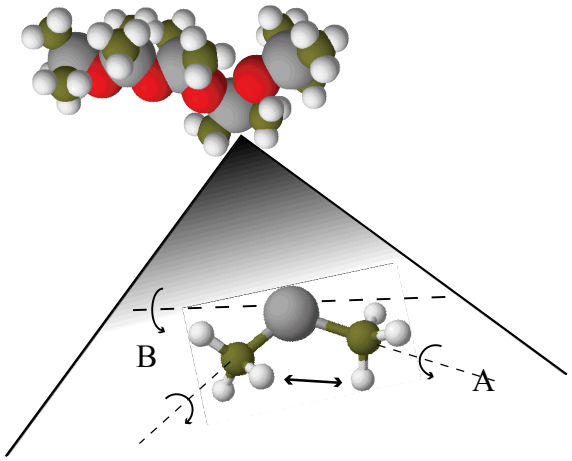

Figure 2. NMR pulse sequences used in this study. (A) Hahn Spin-echo pulse sequence; (B) refocused MQ-NMR pulse sequence.

(A)

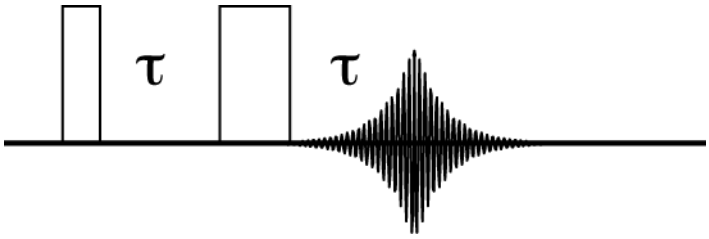

(B)

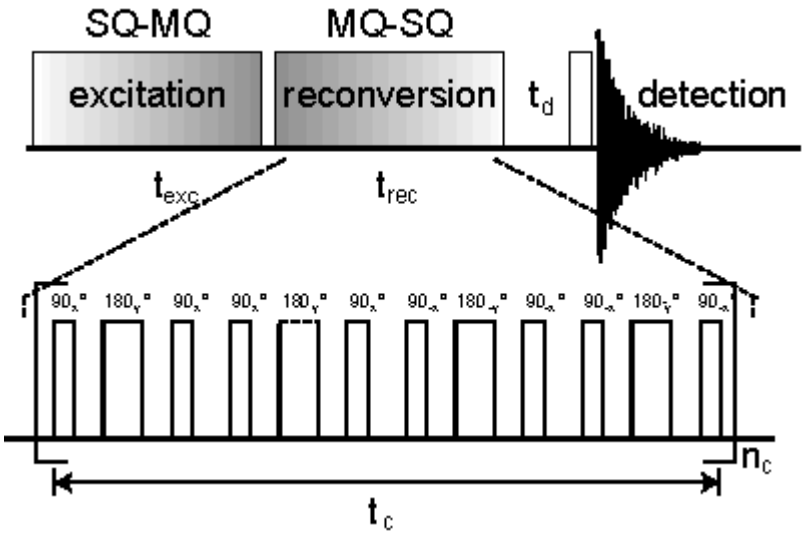

Figure 3. Total Ion Chromatagrams from SPME-GC/MS analysis of offgassing signatures from TR55 samples exposed to γ-radiaton. Sampling protocols are described in the text. Species are identified in Table 1.

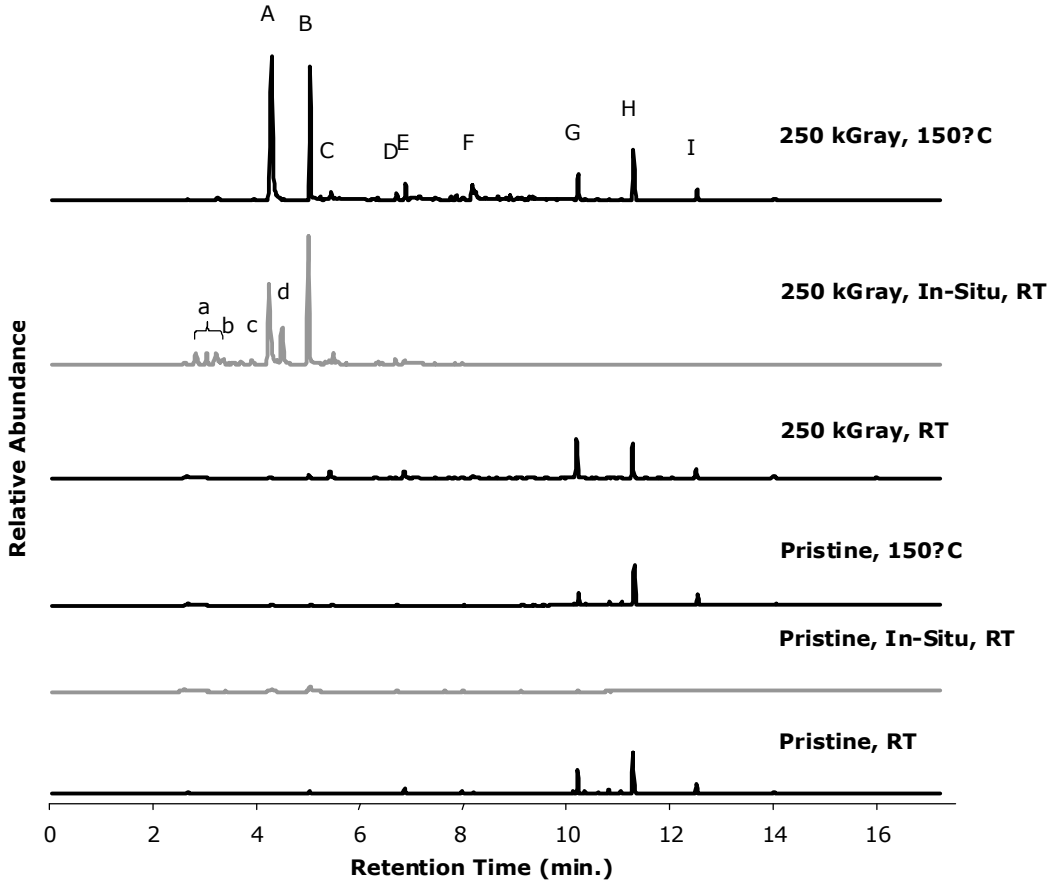

Figure 4. Results of (A) solvent swelling in toluene and (B) DMA studies on TR55 samples exposed to increasing cumulative doses of Co-60 γ-radiation. Details of the two phase solvent swelling approach are described in the text.

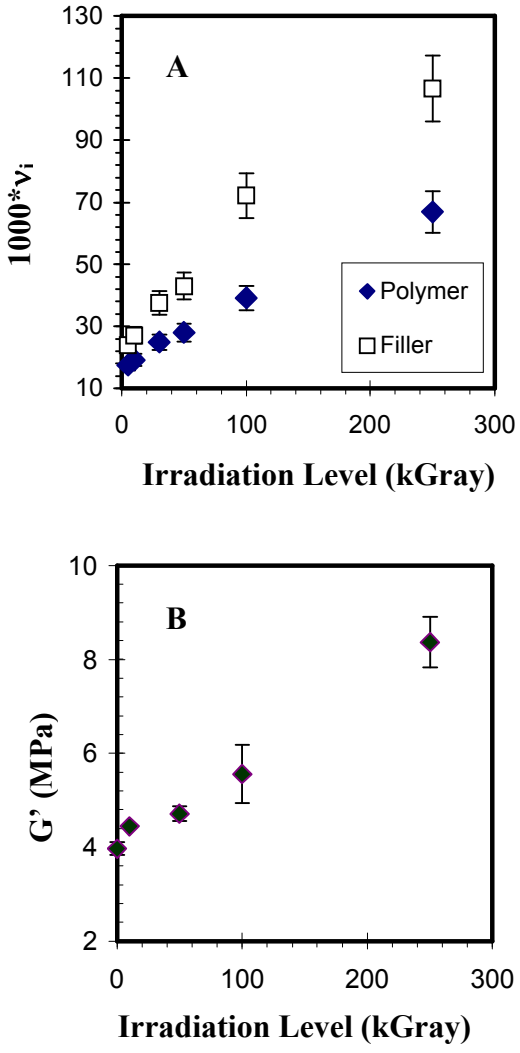

Figure 5. (A) Spin-echo decay curves for TR55 silicone elastomer exposed to increasing doses of γ-radiation. Increased decay rate is indicative of dominant crosslinking reactions. Results of deconvolution of spin-echo decay curves in Figure 5: (B) effective spin-echo decay time constant ($1T_2$ = 1/time to reach 1/e of initial intensity) as a function of cumulative dose; (C) mean square residual dipolar coupling obtained from fitting spin-echo decay curves in Figure 5 to equation {4} as a function of cumulative dose.

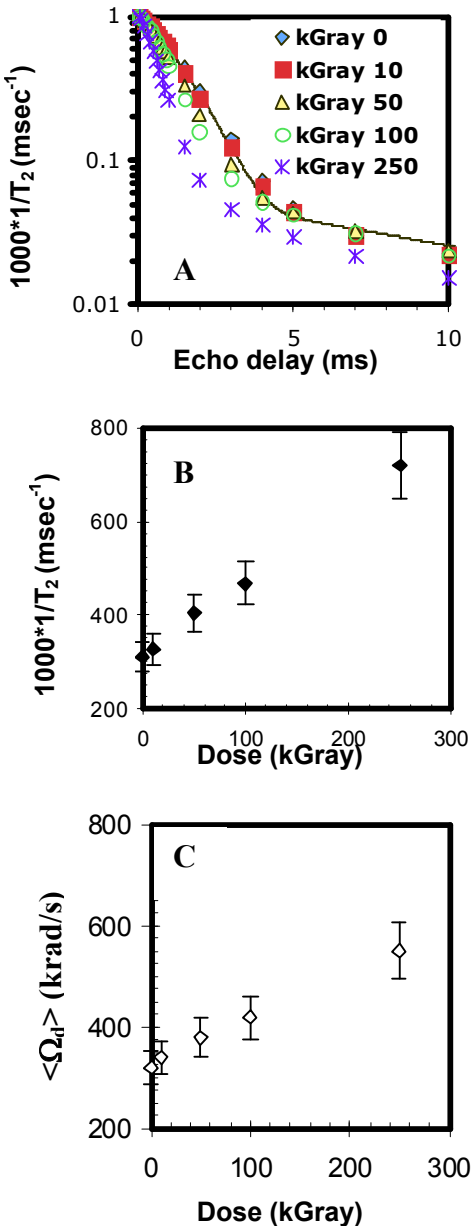

Figure 6. Charlseby-Pinner plot of sol-fraction (as deterimined from NMR analysis) as a function of inverse cumulative dose. Nonlinearity indicates a non-random distribution of chain lengths in the network structure and extrapolation to infinite dose indicates a ratio of chain scission to crosslinking (G_s/G_x)of 0.38 ± 0.02.

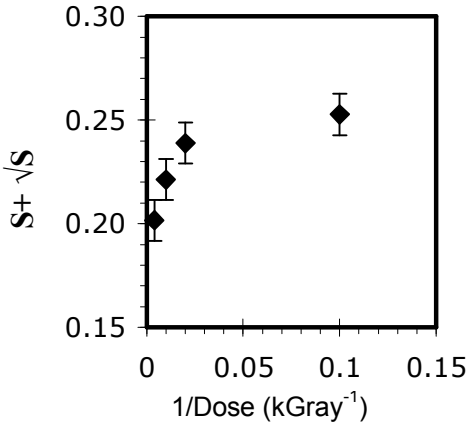

Figure 7: Results of DSC analysis of TR55 samples subject to exposure to g-radiation from a Co-60 source: (A) Heat of melting as measured at melt temperature; (B) Melt temperature.

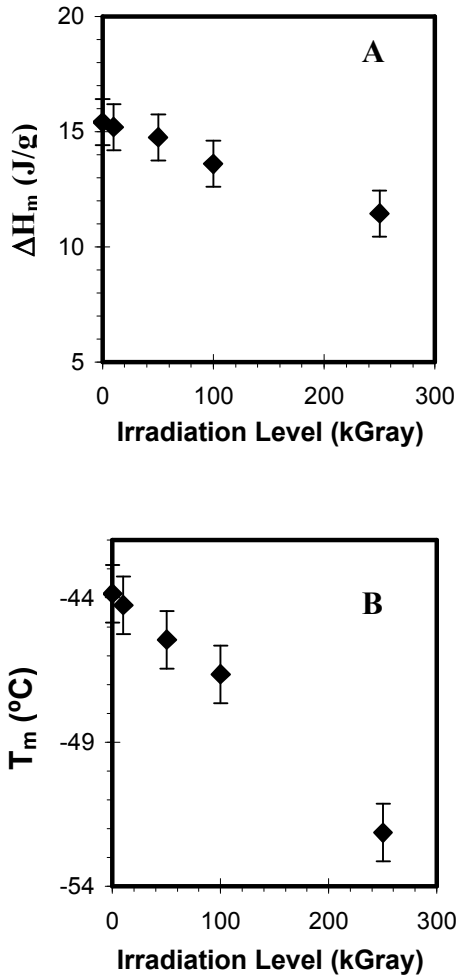

Figure 8. Normalized MQ-NMR growth curves obtained by the pulse sequence described in Figure 2 for TR55 silicone samples exposed to increasing doses of γ-radiation. Solid curves are fits of experimental data to two Gaussian distributions of $\langle\Omega_d\rangle$ as described in equation {6}. Increased growth rate is indicative of increase crosslinking due to effects of radiation.

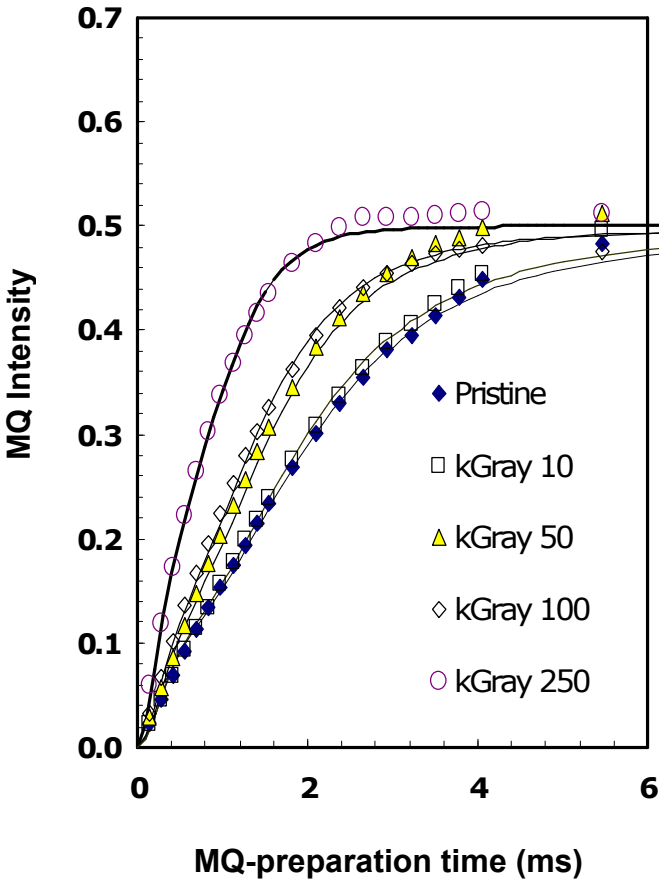

Figure 9. Histograms of Population vs. $<\Omega_d>$ from fits of growth curves to equation {6}. Histograms are offset vertically for clarity and are normalized so that the total area under the curves are constant for all histograms.

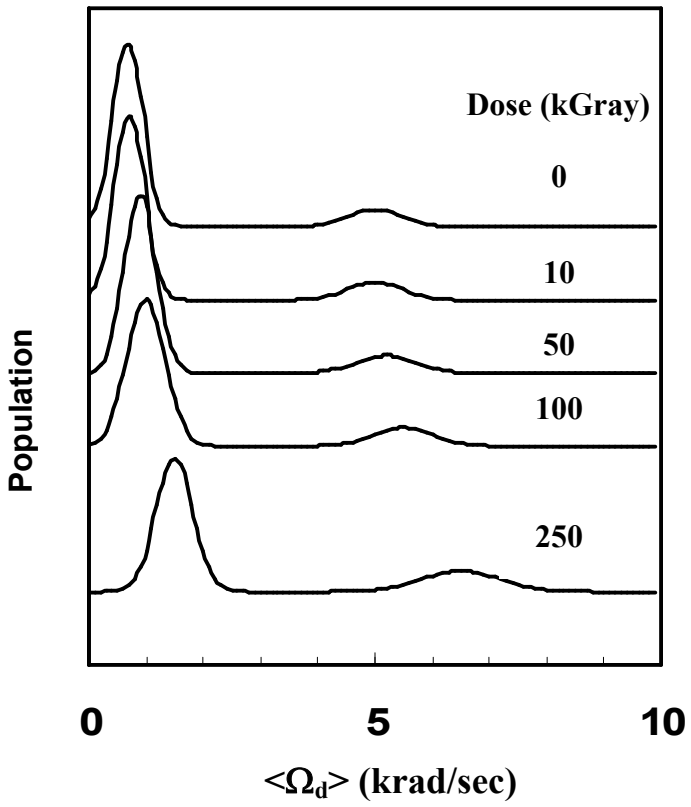

Figure 10: Results of deconvolution of histograms shown in Figure 9: (A) mean $<\Omega_d>$ for both domains as a function of cumulative dose; (B) fractional population (X_{low}) in domain with lower $<\Omega_d>$.